High efficiency solution-processed two-dimensional small molecule organic solar cells obtained via low-temperature thermal annealing — Source link [↗]

Zhengkun Du, Weichao Chen, Chen Yanhua, Chen Yanhua ...+6 more authors

Institutions: Chinese Academy of Sciences, Ocean University of China

Related papers:

- Solution-Processed Organic Solar Cells Based on Dialkylthiol-Substituted Benzodithiophene Unit with Efficiency near 10%

- Solution-processed and high-performance organic solar cells using small molecules with a benzodithiophene unit.

- Small Molecules Based on Benzo[1,2-b:4,5-b′]dithiophene Unit for High-Performance Solution-Processed Organic Solar Cells

- Solution-processed small-molecule solar cells: breaking the 10% power conversion efficiency

- Small molecule semiconductors for high-efficiency organic photovoltaics

Share this paper: [f] [𝕏] [in] [✉]

PAPER

High efficiency solution-processed two-dimensional small molecule organic solar cells obtained *via* low-temperature thermal annealing†

Zhengkun Du,[ab] Weichao Chen,[a] Yanhua Chen,[ac] Shanlin Qiao,[a] Xichang Bao,[a] Shuguang Wen,[a] Mingliang Sun,[c] Liangliang Han[a] and Renqiang Yang*[a]

A new two-dimensional (2D) organic small molecule, **DCA3T(T-BDT)**, was designed and synthesized for solution-processed organic solar cells (OSCs). **DCA3T(T-BDT)** exhibited a deep HOMO energy level (−5.37 eV) and good thermal stability. The morphologies of the **DCA3T(T-BDT)**:[6,6]-phenyl-C61-butyric acid methyl ester ($PC_{61}BM$) blends were investigated by atomic force microscopy and the crystallinity was explored by X-ray diffraction (XRD) and 2D grazing incidence wide-angle X-ray scattering (GIWAXS), respectively. The morphologies of the blends were strongly influenced by the blend ratio of **DCA3T(T-BDT)**:$PC_{61}BM$ and annealing temperature. The effect of thermal annealing on the photovoltaic performance of **DCA3T(T-BDT)**-based small molecule organic solar cells (SMOSCs) was studied in detail. When **DCA3T(T-BDT)** was used as a donor with $PC_{61}BM$ as an acceptor, high efficiency SMOSCs with a power conversion efficiency of 7.93%, a high V_{oc} of 0.95 V, J_{sc} of 11.86 mA cm^{-2} and FF of 0.70 were obtained by a thermal annealing process at only 60 °C, which offers obvious advantages for large scale production compared with solvent additive or interfacial modification treatment.

1. Introduction

Over the past two decades, organic solar cells (OSCs) as a promising renewable energy source have attracted considerable attention of chemical, material and physical scientists because of their low cost, light weight, and large area fabrication on flexible substrates.[1–9] At present, the power conversion efficiency (PCE) of bulk heterojunction (BHJ) OSCs based on low band gap conjugated polymer is over 9% using an inverted device architecture.[10] As an alternative candidate for polymer solar cells, small molecule organic solar cells (SMOSCs) have recently achieved great development, and PCE of over 8% have been realized through carefully modifying the molecular structure and using additives.[11,12] Although PCE is still relatively lower than that of polymer solar cells, SMOSCs have a better prospect of industrialization due to their unique advantages of well-defined molecular structure, synthetic reproducibility, mono-dispersity, and convenient energy level control.[13–22] Thus, further work on designing new small molecules and gaining a better understanding of the molecular structure-function relationships are needed for their future commercial applications.

Compared to their polymeric counterparts,[23–25] in most cases, SMOSCs have relatively low fill factor (FF) and short circuit current density (J_{sc}) due to their poorer film formation ability and this has become the main hindrance for developing high performance devices.[26] To date, conjugated organic small molecules with wide absorption, high hole mobility, as well as appropriate miscibility with the fullerene acceptor to form uniform interpenetrating networks were designed and synthesized for high efficiency SMOSCs.[17,27] Among the vast variety of the developed electron-donating materials for OSCs, two-dimensional (2D) alkylthiophene substituted benzo[1,2-*b*:4,5-*b*′]-dithiophene (BDT) has been proved to be a promising material for photovoltaic applications.[28–30] The incorporation of thiophene side chains could extend the vertical π–π conjugation and promote π–π stacking in the solid state.[31] This extended conjugated structure is beneficial in improving charge transport and correspondingly achieve a high J_{sc}.[31,32] Compared with a one-dimensional (1D) BDT-based conjugated polymer,[6] the 2D BDT-based polymer generally represents a higher open-circuit voltage (V_{oc}) in the organic solar cell due to its lower highest occupied molecular orbital (HOMO) levels.[33,34] Hou *et al.* reported a series of copolymers based on 2D BDT derivatives, which showed excellent photovoltaic performance with PCEs of over 7%.[31,35] Considering the great progress that has been achieved in polymer OSCs using 2D BDT derivatives, the 2D BDT unit is a promising donor material for SMOSCs.[12,15,36] Therefore,

[a]CAS Key Laboratory of Bio-based Materials, Qingdao Institute of Bioenergy and Bioprocess Technology, Chinese Academy of Sciences, Qingdao 266101, China. E-mail: yangrq@qibebt.ac.cn
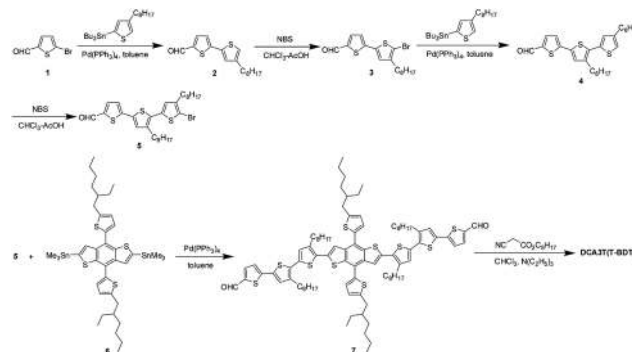
[b]University of Chinese Academy of Sciences, Beijing 100049, China

[c]Institute of Materials Science and Engineering, Ocean University of China, Qingdao 266100, China
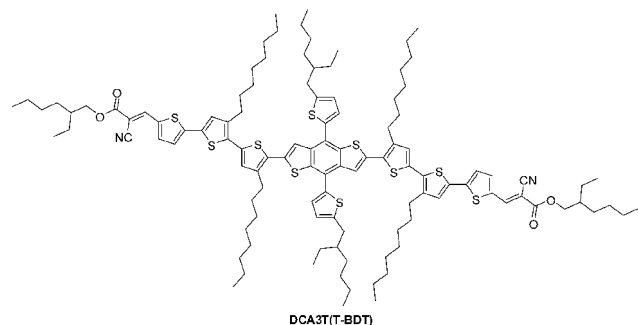
Scheme 1 Chemical structure of **DCA3T(T-BDT)**.

Scheme 2 Synthetic routes towards **DCA3T(T-BDT)**.

novel small molecules with high efficiency would be designed and synthesized if the HOMO and LUMO levels of the 2D BDT-based small molecules could be effectively tuned by employing appropriate electron-withdrawing groups. On the other hand, a suitable method for fabricating the organic solar cells is also crucial for achieving high efficiency. Thermal annealing of BHJ films is one of the most widely used methods for improving the J_{sc} and FF of BHJ OSCs.[37–40] However, as the thermal annealing temperature increases, the V_{oc} of SMOSCs sometimes significantly decreases.[38] Given the effect of thermal annealing on the morphology and crystallinity of the film, a delicate balance between V_{oc}, J_{sc} and FF could be achieved by annealing at a low temperature, and a maximum PCE of solution-processed SMOSCs will be achieved.

In view of the aforementioned concerns, we have successfully synthesized a new solution-processed 2D-conjugated organic small molecule, **DCA3T(T-BDT)** (Scheme 1), with 2-ethylhexyl cyanoacetate units as the end-capped blocks and 4,8-bis[5-(2-ethylhexyl)thiophen-2-yl]benzo[1,2-b:4,5-b']-dithiophene as the central core. BHJ OSCs were fabricated using a blend of **DCA3T(T-BDT)** as the donor and $PC_{61}BM$ as the acceptor, with a single layer conventional device architecture of ITO/PEDOT:PSS/**DCA3T(T-BDT)**:$PC_{61}BM$/Ca/Al. The best device exhibited a high PCE of 7.93% after thermal annealing at a low temperature of 60 °C for 10 min, with a high V_{oc} of 0.95 V, J_{sc} of 11.86 mA cm^{-2} and FF of 0.70. To the best of our knowledge, this is the highest PCE for solution-processed SMOSCs without any solvent additive or interfacial modification treatment found in the conventional devices.

2. Results and discussion

2.1 Synthesis and characterization

The detailed synthesis and characterization of **DCA3T(T-BDT)** are given in the experimental section (Scheme 2). The key precursor **7** was synthesized using a Pd(PPh$_3$)$_4$-catalyzed Stille coupling reaction between 4',4''-dioctyl-2,2':5',2''-trithiophene-5-carbaldehyde (**5**) and 2,6-bis(trimethyltin)-4,8-bis(5-(2-ethyl-hexyl)thiophen-2yl-)benzo[1,2-b:4,5-b']dithiophene (**6**) in refluxing toluene under argon for 2 days. The target small molecule **DCA3T(T-BDT)** was obtained through the Knoevenagel condensation of intermediate **7** with 2-ethylhexyl cyanoacetate using triethylamine as the catalyst in anhydrous chloroform (CHCl$_3$)

for 40 h. The **DCA3T(T-BDT)** was fully characterized by NMR spectroscopy, mass spectrometry, electrochemistry, high performance liquid chromatography with UV-detection (HPLC-UV), thermogravimetric analysis (TGA) and optical spectroscopy. **DCA3T(T-BDT)** possesses good solubility at room temperature in common organic solvents, such as toluene, chlorobenzene, o-dichlorobenzene, dichloromethane (CH$_2$Cl$_2$) and CHCl$_3$, due to eight solubilizing alkyl side chains.

2.2 Thermal stability

TGA and differential scanning calorimetry (DSC) were used to investigate the thermal properties of the small molecule. As shown in Fig. 1, the TGA curve of **DCA3T(T-BDT)** indicates a good thermal stability with onset decomposition temperature with a 5% weight loss (T_d) occurring at 389 °C under an nitrogen atmosphere. The thermal stability of **DCA3T(T-BDT)** is high enough to ensure the photovoltaic device fabrication. As shown in Fig. S2,† the main melting endotherm occurs at 163.7 °C, and upon cooling **DCA3T(T-BDT)** exhibits a major crystallization exotherm at 133.5 °C, indicating that this small molecule has an obvious tendency to crystallize.
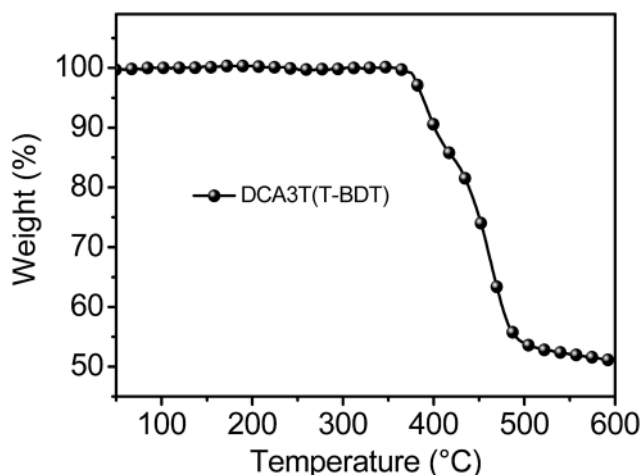
Fig. 1 TGA plot of **DCA3T(T-BDT)** with a heating rate of 10 °C min^{-1} under nitrogen atmosphere.

2.3 Optical and electrochemical properties

UV-vis absorption spectra of **DCA3T(T-BDT)** were investigated in CHCl$_3$ solution and as a thin film, as shown in Fig. 2a. **DCA3T-(T-BDT)** exhibited a broad absorption range covering 300–700 nm wavelengths in the solid state. In solution, **DCA3T(T-BDT)** has a maximal absorption (λ_{max}) peak at 499 nm corresponding to the intermolecular charge transfer (ICT) interaction between D and A moieties.[41,42] In comparison with its absorption spectrum in solution, the absorption spectrum of **DCA3T(T-BDT)** as a thin film shows a remarkable red-shifted λ_{max} at 573 nm with a shoulder peak at 620 nm, indicating that a strong intermolecular π–π interaction exists in the solid state due to the improved planar construction of the 2D side chains. The optical band gap (E_g^{opt}) value of **DCA3T(T-BDT)** is about 1.80 eV, which is deduced from the onset (690 nm) of absorption in the thin film.

Density functional theory (DFT) calculations were employed to investigate the electronic structure and geometry of **DCA3T(T-BDT)**, and the corresponding results are shown in Fig. 3. The electron density of HOMO was mainly delocalized over the central BDT core, and the electron density of the LUMO was concentrated on the 2-ethylhexyl cyanoacetate groups, demonstrating that an electron can transfer from the central BDT group to the end-capped blocks during an electronic excitation process.[43] From the DFT calculations, the HOMO and LUMO energies of **DCA3T(T-BDT)** were found to be −4.98 eV and −2.82 eV, respectively. The electrochemical behavior of **DCA3T(T-BDT)** was investigated by cyclic voltammetry (CV). As shown in Fig. 2b, the onset oxidation potential for the small molecule was 0.95 V *versus* a saturated calomel electrode (SCE).
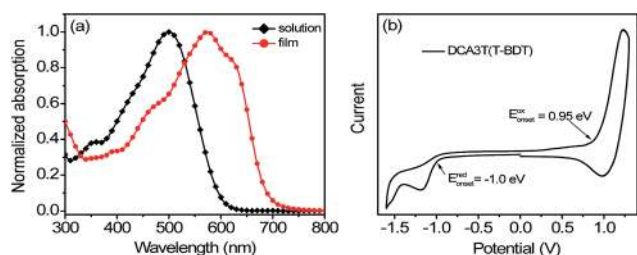
The corresponding HOMO energy level of **DCA3T(T-BDT)** was determined to be −5.37 eV. The LUMO energy levels of **DCA3T(T-BDT)** was estimated to be around −3.42 eV from the onset reduction potential. This fairly suitable HOMO energy level conveys that a high V_{oc} of SMOSCs based on **DCA3T-(T-BDT)** blended with PC$_{61}$BM could be expected.[31] The LUMO energy level difference (>0.3 eV) between the donor and acceptor (PC$_{61}$BM) is large enough for the separation of the excitons,[44–47] which is very useful for increasing the short-circuit current in **DCA3T(T-BDT)**-based OSCs.

2.4 Hole mobility

The high carrier charge mobility is important for effective photovoltaic active layer materials, which would facilitate charge exciton separation from the donor–acceptor interface, carrier transport to the electrodes and reduce recombination.[15] The carrier charge mobility of **DCA3T(T-BDT)** was investigated by employing organic field-effect transistors (OFETs) and vertical diodes. **DCA3T(T-BDT)** exhibited a typical p-type semiconductor behavior (Fig. 4), and the hole mobility was around 0.03 cm^2 V^{-1} s^{-1}, calculated according to the transfer characteristic curve. In the vertical direction, the hole mobility was measured by the space-charge limit current (SCLC)[48–50] model with a typical device structure of ITO/PEDOT:PSS/**DCA3T-(T-BDT)**/Au. SCLC is described by the equation $J_{SCLC} = (9/8) \varepsilon_0 \varepsilon_r \mu_h ((V^2)/(L^3))$, where J stands for current density, ε_0 is the permittivity of free space, ε_r is the relative dielectric constant of the transport medium, μ_h is the hole mobility, V is the internal potential in the device and L is the thickness of the active layer. The hole mobility of **DCA3T(T-BDT)** was about 1.2×10^{-4} cm^2 V^{-1} s^{-1}, calculated using the SCLC model (Fig. S4†).

2.5 Photovoltaic properties

The BHJ solar cells with a conventional architecture of ITO/PEDOT:PSS/**DCA3T(T-BDT)**:PC$_{61}$BM/Ca/Al using PC$_{61}$BM as the acceptor were fabricated to explore the photovoltaic performance of **DCA3T(T-BDT)**. The detailed device fabrication and measurements are described in the experimental section. First, after thickness optimization, the relative ideal thickness of active layer was around 90 nm for **DCA3T(T-BDT)**-based OSCs. The effect of different D/A blend ratios on the performance of SMOSCs based on **DCA3T(T-BDT)** and PC$_{61}$BM was investigated, and the corresponding results are collected in Table 1. With an increase of the D/A blend ratio from 1 : 1 to 4 : 1, V_{oc} slightly

Fig. 2 (a) UV-vis absorption spectra of **DCA3T(T-BDT)** in CHCl$_3$ solution and as a solid thin film. (b) Cyclic voltammogram of **DCA3T-(T-BDT)** in 0.1 M Bu$_4$NPF$_6$-acetonitrile solution at a scan rate of 100 mV s^{-1}.
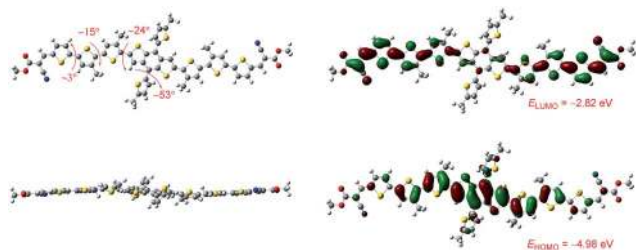

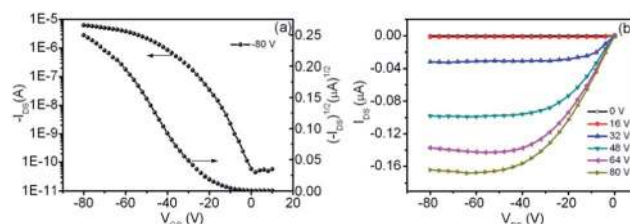Fig. 3 Optimized molecular geometries and frontier molecular orbitals (isovalue surface 0.02 au) using DFT evaluated at the B3LYP/6-31G(d) level of theory.

Fig. 4 (a) Transfer and (b) output characteristics (V_{DS} = −80 V) for a typical **DCA3T(T-BDT)**-based OFET device.

15906 | *J. Mater. Chem. A*, 2014, **2**, 15904–15911

This journal is © The Royal Society of Chemistry 2014

Table 1 The photovoltaic performance of SMOSCs based on DCA3T(T-BDT):PC$_{61}$BM before and after thermal annealing with different blend ratio

D : A (w/w)	Thermal annealing	V_{oc} (V)	J_{sc} (mA cm^{-2})	FF	PCE$_{max}$ (PCE$_{ave}$[a]) (%)
1 : 1	No	0.95	7.64	0.42	3.04 (2.90)
	60 °C	0.94	9.76	0.52	4.78 (4.61)
2 : 1	No	0.96	11.21	0.60	6.55 (6.27)
	60 °C	0.95	11.33	0.67	7.25 (7.04)
3 : 1	No	0.97	11.22	0.66	7.19 (6.98)
	40 °C	0.96	11.27	0.68	7.36 (7.16)
	60 °C	0.95	11.86	0.70	7.93 (7.79)
	80 °C	0.95	11.16	0.68	7.21 (7.03)
4 : 1	No	0.98	10.26	0.57	5.98 (5.79)
	60 °C	0.95	9.16	0.70	11.11 (5.97)

[a] The average PCE was obtained from over 10 devices.

increased, but J_{sc} and FF first increased and then gradually decreased. The optimized device made from the **DCA3T(T-BDT)** blended with PC$_{61}$BM (3 : 1, w/w) shows the highest PCE of 7.19%, with a V_{oc} of 0.97 V, J_{sc} of 11.22 mA cm^{-2} and FF of 0.66. The high J_{sc} could be partly ascribed to the better absorption of **DCA3T(T-BDT)** and the suitable energy matching and larger V_{oc} agrees with its deeper HOMO energy level (−5.37 eV). The device performance is consistent with the morphologies of the films with different ratio, which are shown in the Fig. 6a–d. The domain in the films is gradually increasing with an increase in the D : A ratio, and the domain boundary is reduced. A good interpenetrating network could be formed at the ratio of 3 : 1 (D : A) with relatively low boundary density, which is in favor of the improvement of J_{sc} and FF.

To further improve the photovoltaic performance of SMOSCs based on **DCA3T(T-BDT)** and PC$_{61}$BM, thermal annealing was employed. The device parameters with different annealing temperatures are summarized in Table 1. The performance of the devices were improved by thermal annealing with higher J_{sc} and FF compared to the devices as casted. The optimized device based on the **DCA3T(T-BDT)**/PC$_{61}$BM (3 : 1, w/w) blend shows a PCE of 7.93%, V_{oc} of 0.95 V, J_{sc} of 11.86 mA cm^{-2} and FF of 0.70 after thermal annealing at only 60 °C (Fig. 5a). The performance of the devices with different ratios could also be enhanced after annealing, as shown in the Table 1. Therefore, thermal annealing at relatively low temperature is a good method to improve the PCE of the devices and has obvious advantages for

large scale production. It is worth noting that all the devices exhibited high V_{oc} (0.94–0.98 V), which were almost insensitive to the annealed temperature and the D/A weight ratios. The J–V curves of the devices with different D/A blend ratios under the illumination of AM 1.5G (100 mW cm^{-2}) are shown in Fig. S3.† As a result, **DCA3T(T-BDT)** would be a promising donor material for high efficiency SMOSCs.

The EQE curve of the optimized device covered a broad wavelength range of 310–700 nm with a maximum value of 70% at 569 nm as shown in Fig. 5b. After thermal annealing at 60 °C, the photoresponse is enhanced at the long wavelength region, which may be the contribution of improvement of the crystallization. J_{sc} calculated from the EQE curve is 11.34 mA cm^{-2}, which is consistent with the J_{sc} value obtained from the J–V curve.

2.6 Morphology and structural (X-ray) characterization

The enhanced device performance by the thermal annealing process at low temperature could be partially attributed to a better interpenetrating network.[27] The morphologies of the films with the **DCA3T(T-BDT)**:PC$_{61}$BM (3 : 1, w/w) blend annealing at different temperatures are given in Fig. S5.† The films after annealing show a lower root mean square compared to the pristine ones. Upon increasing the annealing temperature from 40 to 80 °C, the domain boundary intensity gradually reduced, which would decrease the trap state density existing in the boundary and therefore reduce the recombination current and improve the transport and collection of the carrier charge.[51] This may also be an important reason for the improvement of J_{sc} and FF in this work. The morphologies of films with different D : A ratio after annealing at 60 °C are given in Fig. 6e–h. All films show a lower boundary intensity compared to their films as casted. Therefore, it is believed that thermal annealing at relatively low temperature may be an effective method to enhance the performance of devices by reducing the boundary intensity.

To further understand the performance difference of **DCA3T(T-BDT)**-based SMOSCs before and after thermal annealing at 60 °C, the crystallinity of the **DCA3T(T-BDT)**
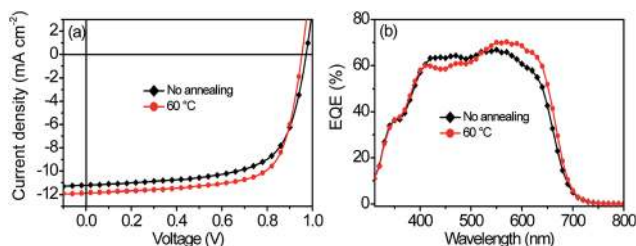

Fig. 5 (a) J–V characteristics and (b) EQE curves of the devices based on DCA3T(T-BDT):PC$_{61}$BM before and after thermal annealing at 60 °C with a blend ratio of 3 : 1.
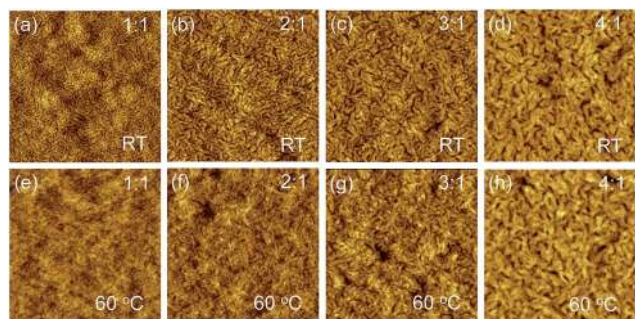
This journal is © The Royal Society of Chemistry 2014

J. Mater. Chem. A, 2014, 2, 15904–15911 | 15907

Fig. 6 Tapping mode AFM height images (4 μm × 4 μm) of **DCA3T(T-BDT)**:PC$_{61}$BM blend films with different D/A ratios before (top: a–d) and after (bottom: e–h) thermal annealing at 60 °C.

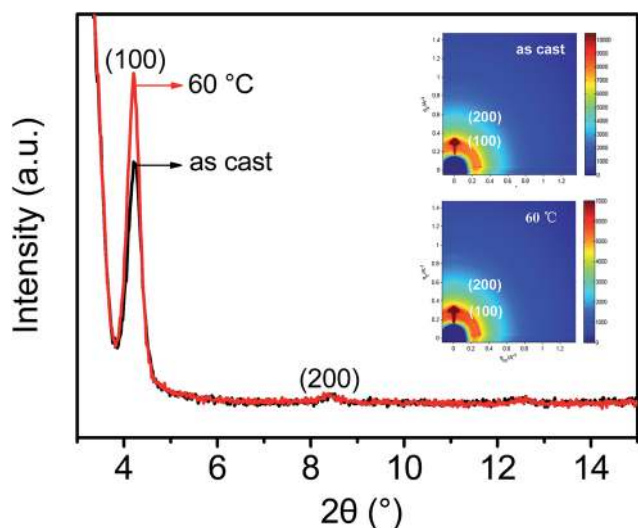**Fig. 7** XRD patterns of **DCA3T(T-BDT)** film spin-coated from CHCl$_3$ solution before and after thermal annealing at 60 °C. The insets are the corresponding 2D GIWAXS images.

blend films was investigated by X-ray diffraction (XRD) and two-dimensional (2D) grazing incidence wide-angle X-ray scattering (GIWAXS), respectively. As shown in Fig. 7, the diffraction peak of the annealing film remained at the same position, and the intensity was obviously enhanced. Both of the films show an evident diffraction peak (100) at $2\theta = 4.2°$, corresponding to a d_{100}-spacing value of 21.0 Å. The second-order diffraction peak (200) at $2\theta = 8.4°$, corresponding to a d_{200}-spacing value of 10.5 Å was also clearly observed, indicating the high crystallinity of **DCA3T(T-BDT)** in the solid thin film. The stronger diffraction peak of the annealing film compared to the pristine one reveals that the low temperature annealing would improve the ordering in the donor phase.[52,53] The 2D GIWAXS patterns also indicate a well-ordered crystal structure throughout the corresponding thin film. The high crystallinity could increase the carrier mobility, which would be benefit for the transport and collection of the carrier,[54] thus leading to a higher J_{sc} and FF.

3. Conclusion

In conclusion, a new low band gap and 2D-conjugated organic small molecule, **DCA3T(T-BDT)**, was designed and synthesized for solution-processed organic solar cells. **DCA3T(T-BDT)** exhibited good solubility, thermal stability, crystallinity and a deeper HOMO energy level of −5.37 eV. High efficiency small molecule organic solar cell with a power conversion efficiency of 7.93%, a high V_{oc} of 0.95 V, J_{sc} of 11.86 mA cm^{-2} and FF of 0.70 was obtained by thermal annealing process at only 60 °C. Hence, this encouraging result reveals a prospective strategy for a new 2D heterocyclic core in constructing donor–acceptor type small molecules for high performance organic solar cells.

4. Experimental section

4.1 Materials, instruments and characterization

All starting materials and reagents were purchased from commercial sources and used without further purification, unless otherwise mentioned. Toluene was distilled over sodium in the presence of benzophenone to remove water. CHCl$_3$ and CH$_2$Cl$_2$ were distilled over calcium hydride (CaH$_2$).

^{1}H and ^{13}C NMR spectra were obtained on a Bruker Advance III 600 spectrometer with tetramethylsilane (TMS, $\delta = 0$ ppm) as an internal standard. UV-vis absorption spectra were obtained on a Hitachi U-4100 spectrophotometer. High resolution mass spectra were recorded under APCI mode on a Bruker Maxis UHR TOF spectrometer. TGA and DSC were carried on SDT Q600 simultaneous DSC-TGA instrument and Perkin Elmer diamond differential scanning calorimeter, respectively. Cyclic voltammetry (CV) measurements were taken on a CHI660D electrochemical workstation. Moreover, CV experiments were carried out at room temperature with a conventional three-electrode system using a platinum wire as the counter electrode, a saturated calomel electrode (SCE) as the reference electrode, and a glassy carbon electrode as the working electrode. A solution of tetrabutylammonium phosphorus hexafluoride (Bu$_4$NPF$_6$, 0.1 M) in acetonitrile was used as the supporting electrolyte, at a scan rate of 100 mV s^{-1}. Ferrocene/ferrocenium (Fc/Fc$^+$) was used as the internal standard (the energy level of Fc/Fc$^+$ is −4.8 eV under vacuum) and the formal potential of Fc/Fc$^+$ was measured as 0.38 V $vs.$ SCE. HPLC-UV was carried on a Waters 1525 high performance liquid chromatography with UV detection.

Density functional theory (DFT) calculations were performed using the Gaussian 09 program suite at the B3LYP/6-31G(d) level to investigate the electronic structure of the molecule in the gas phase.[55–58] All the alkyl side chains were replaced with methyl groups to reduce the computational cost. The optimized molecular structure was confirmed to be in a stable local minimum of the ground state potential energy surface by computing the vibrational frequencies at the same level of theory.

OFET was fabricated using n-type heavily doped Si as the gate with a 300 nm thermally oxidized SiO$_2$ layer as the gate dielectric (the capacitance was 10 nF cm^{-2}). The film was prepared by spin-coating the solution (6 mg mL^{-1} in CHCl$_3$) on

octadecyltrichlorosilane (OTS)-treated SiO_2/Si. The Au source and drain electrodes were deposited on the film through a shadow mask with a length of 31 μm and a width of 273 μm. Measurements were performed using a 4200 semiconductor parameter analyzer in air.

4.2 Fabrication of DCA3T(T-BDT)-based organic solar cells

SMOSCs were fabricated with a structure of ITO/PEDOT :PSS/ **DCA3T(T-BDT)**:$PC_{61}BM$/Ca/Al using a conventional solution spin-coating process. The ITO-coated glass substrates were cleaned by ultrasonic treatment in detergent, deionized water, acetone and isopropyl alcohol under ultrasonication for 20 min. A thin layer of PEDOT:PSS was spin-coated (4000 rpm, *ca.* 40 nm thick) onto the ITO surface. After being baked at 150 °C for 20 min, the substrates were transferred into a glove box. Subsequently, the active layer was spin-coated from different ratio blends of **DCA3T(T-BDT)** and $PC_{61}BM$ in $CHCl_3$ solution at 1500 rpm for 25 s on the ITO/PEDOT:PSS substrate. Finally, a 10 nm Ca layer and 100 nm Al layer were successively deposited onto the active layer under high vacuum by a shadow mask to define the area of 0.1 cm^2 ($<3 \times 10^{-4}$ Pa). The thermal annealing was carried out by placing the completed devices on a digitally controlled hotplate at different temperatures, in an argon-filled glove box.

4.3 Measurement and characterization of devices

The structure of the films was analyzed using grazing incidence X-ray diffraction (GIXRD, Bruker D8 ADVANCE). Surface morphological characterization of the films were carried out by a tapping-mode atomic force microscope (AFM, Agilent 5400). Current density–voltage (*J–V*) characteristics of the devices were analyzed with a Keithley 2420 source measurement unit under simulated 100 mW cm^{-2} (AM 1.5G) irradiation from a Newport solar simulator. Light intensity was calibrated with a standard silicon solar cell. Further, the external quantum efficiencies (EQE) of solar cells were analyzed using a certified Newport incident photon conversion efficiency (IPCE) measurement system.

4.4 Synthesis

All coupling reactions were conducted under purified argon and monitored by Merck silica-gel thin-layer chromatography (TLC). 2-(Tributylstannyl)-4-octylthiophene and 2,6-bis(trimethyltin)-4,8-bis(5-(2-ethylhexyl)thiophen-2yl-)benzo[1,2-*b*:4,5-*b'*]dithiophene (**6**) were synthesized according to the literature procedures.[59,60]

4′-Octyl-2,2′-bithiophene-5-carbaldehyde (2). In a 100 mL flame-dried flask, 2-(tributylstannyl)-4-octylthiophene (8.90 g, 18.32 mmol), 5-bromo-2-thiophene-carbaldehyde (3.18 g, 16.5 mmol) and Pd(PPh$_3$)$_4$ (0.76 g, 0.66 mmol) were dissolved in anhydrous degassed toluene (60 mL). The mixture was slowly heated up to 110 °C and stirred at this temperature overnight under an argon atmosphere. After cooling down to the room temperature, the mixture was poured into water and extracted three times with CH_2Cl_2. The combined organic phase was dried over anhydrous Na_2SO_4 and concentrated under vacuum. The crude residue was purified by column chromatography on silica gel using petroleum/CH_2Cl_2 as eluent. After removing the solvents, a light yellow solid compound **2** (2.86 g, 57%) was obtained.

^{1}H NMR (600 MHz, CDCl$_3$), δ (ppm): 9.85 (s, 1H), 7.65 (d, 1H), 7.21 (d, 1H), 7.19 (d, 1H), 6.95 (d, 1H), 2.60 (t, 2H), 1.63 (m, 2H), 1.35–1.25 (m, 10H), 0.88 (t, 3H). ^{13}C NMR (150 MHz, CDCl$_3$), δ (ppm): 182.53, 147.68, 144.79, 141.45, 137.35, 135.63, 127.46, 123.91, 121.93, 31.87, 30.40, 30.38, 29.39, 29.27, 29.25, 22.67, 14.11.

5′-Bromo-4′-octyl-2,2′-bithiophene-5-carbaldehyde (3). In a 250 mL flask, compound **2** (2.45 g, 8.0 mmol) was dissolved in a mixture of CHCl$_3$ (60 mL) and acetic acid (60 mL). Under argon atmosphere and dark against light, *N*-bromosuccinimide (NBS) (1.43 g, 8.0 mmol) was added to the solution in small portions and the reaction mixture was stirred for 8 h at room temperature. The mixture was diluted with water and extracted with CH_2Cl_2 three times. The combined organic phase was dried over anhydrous Na$_2$SO$_4$ and the solvent was removed by rotary evaporator. The crude product was purified by column chromatography on silica gel using petroleum/CH_2Cl_2 as eluent. After evaporating the solvent under vacuum, compound **3** (2.20 g, 72%) was obtained as a yellow solid.

^{1}H NMR (600 MHz, CDCl$_3$), δ (ppm): 9.84 (s, 1H), 7.62 (d, 1H), 7.13 (d, 1H), 7.02 (s, 1H), 2.53 (t, 2H), 1.58 (m, 2H), 1.33–1.25 (m, 10H), 0.88 (t, 3H). ^{13}C NMR (150 MHz, CDCl$_3$), δ (ppm): 182.37, 146.25, 143.66, 141.72, 137.22, 135.39, 126.75, 124.03, 110.96, 31.86, 29.60, 29.52, 29.34, 29.22, 29.20, 22.67, 14.12.

4′,4″-Dioctyl-2,2′:5′,2″-trithiophene-5-carbaldehyde (4). In a 100 mL flame-dried flask, compound **3** (2.18 g, 5.65 mmol), 2-(tributylstannyl)-4-octylthiophene (3.29 g, 6.78 mmol) and Pd(PPh$_3$)$_4$ (0.19 g, 0.17 mmol) were dissolved in anhydrous degassed toluene (45 mL). The mixture was heated at 110 °C overnight under an argon atmosphere. After cooling down to the room temperature, the mixture was poured into water and extracted with CH_2Cl_2 three times. The combined organic phase was dried over anhydrous Na$_2$SO$_4$ and concentrated under vacuum. The crude residue was purified by column chromatography on silica gel using petroleum/CH_2Cl_2 as eluent to obtain compound **4** (1.69 g, 60%) as a red solid.

^{1}H NMR (600 MHz, CDCl$_3$), δ (ppm): 9.84 (s, 1H), 7.64 (d, 1H), 7.19 (d, 1H), 7.17 (s, 1H), 6.99 (d, 1H), 6.93 (s, 1H), 2.73 (t, 2H), 2.60 (t, 2H), 1.67–1.61 (m, 4H), 1.40–1.27 (m, 20H), 0.88 (m, 6H). ^{13}C NMR (150 MHz, CDCl$_3$), δ (ppm): 182.39, 147.15, 143.87, 141.40, 140.51, 137.40, 134.84, 133.28, 133.11, 129.00, 127.75, 123.85, 120.79, 31.90, 31.88, 30.50, 30.46, 30.43, 29.52, 29.44, 29.38, 29.34, 29.30, 29.28, 29.26, 22.68, 14.12.

5″-Bromo-4′,4″-dioctyl-2,2′:5′,2″-trithiophene-5-carbaldehyde (5). In a 250 mL flask, compound **4** (1.67 g, 3.33 mmol) was dissolved in a mixture of CHCl$_3$ (50 mL) and acetic acid (50 mL). Under argon atmosphere and dark against light, NBS (0.62 g, 3.50 mmol) was added to the solution in small portions, and the reaction mixture was stirred for 6 h at room temperature. The mixture was diluted with water and extracted with CH_2Cl_2 three times. The organic phase was dried over Na$_2$SO$_4$ and the solvent was removed under vacuum. The crude product was purified by

column chromatography on silica gel with petroleum/CH_2Cl_2 as eluent to obtain compound **5** (1.59 g, 82%) as an orange solid.

^{1}H NMR (600 MHz, CDCl$_3$), δ (ppm): 9.86 (s, 1H), 7.66 (d, 1H), 7.21 (d, 1H), 7.16 (s, 1H), 6.85 (s, 1H), 2.70 (t, 2H), 2.57 (t, 2H), 1.66–1.58 (m, 4H), 1.38–1.25 (m, 20H), 0.89 (m, 6H). ^{13}C NMR (150 MHz, CDCl$_3$), δ (ppm): 182.39, 146.80, 142.69, 141.63, 141.03, 137.34, 134.65, 133.63, 132.12, 128.91, 127.23, 124.04, 109.57, 31.89, 31.87, 30.50, 29.67, 29.53, 29.47, 29.38, 29.37, 29.28, 29.25, 22.68, 14.13. MS (UHR-TOF) m/z [M$^+$] = 578.1342 (calcd for $C_{29}H_{39}BrOS_3$, 578.1346).

Compound (7). In a 100 mL well flame-dried flask, compound **5** (1.52 g, 2.62 mmol) and compound **6** (1.04 g, 1.15 mmol) were dissolved in anhydrous toluene (50 mL). After the solution was degassed with argon three times, Pd(PPh$_3$)$_4$ (0.15 g, 0.13 mmol) was added. The reaction mixture was heated at 110 °C for 2 d under an argon atmosphere. After cooling down to room temperature, the mixture was poured into water and extracted with CH_2Cl_2 three times. The combined organic phase was dried over Na$_2$SO$_4$ and concentrated under vacuum. The crude residue was purified by column chromatography on silica gel using petroleum/CH_2Cl_2 as eluent to obtain compound **7** (1.18 g, 65%) as a red solid.

^{1}H NMR (600 MHz, CDCl$_3$), δ (ppm): 9.86 (s, 2H), 7.68 (s, 2H), 7.66 (d, 2H), 7.35 (d, 2H), 7.21 (d, 2H), 7.19 (s, 2H), 7.02 (s, 2H), 6.92 (d, 2H), 2.88 (d, 4H), 2.83 (t, 4H), 2.78 (t, 4H), 1.72–1.65 (m, 10H), 1.43–1.26 (m, 56H), 0.97–0.85 (m, 24H). ^{13}C NMR (150 MHz, CDCl$_3$), δ (ppm): 182.40, 146.94, 145.95, 141.55, 141.53, 140.99, 139.04, 137.38, 136.92, 136.67, 134.46, 133.48, 132.56, 131.53, 129.42, 129.13, 127.78, 125.46, 123.99, 123.36, 121.70, 41.50, 34.31, 32.54, 31.93, 31.87, 30.61, 30.40, 29.61, 29.55, 29.49, 29.47, 29.43, 29.41, 29.35, 29.25, 28.94, 25.73, 23.05, 22.71, 22.67, 14.18, 14.12, 14.11, 10.92. MS (UHR-TOF): calcd for $C_{92}H_{118}O_2S_{10}$ [M]$^+$, 1574.6339; found, 1574.6298.

Compound DCA3T(T-BDT). Under protection of argon, to a stirred solution of CHCl$_3$ (35 mL), triethylamine (0.1 mL) and compound **7** (0.55 g, 0.35 mmol) was added 2-ethylhexyl cyanoacetate (0.8 mL, 3.8 mmol) using a syringe at room temperature. The mixture was stirred for 40 hours under argon. The mixture was diluted with water (45 mL) and extracted with CHCl$_3$ three times. The organic phase was dried over Na$_2$SO$_4$ and the solvent was removed under vacuum. The crude product was purified by column chromatography on silica gel using petroleum/CH_2Cl_2 as eluent to obtain **DCA3T(T-BDT)** (0.51 g, 75%) as a black solid.

^{1}H NMR (600 MHz, CDCl$_3$), δ (ppm): 8.24 (s, 2H), 7.68 (s, 2H), 7.65 (d, 2H), 7.36 (d, 2H), 7.24 (s, 2H), 7.21 (d, 2H), 7.04 (s, 2H), 6.92 (d, 2H), 4.22 (m, 4H), 2.88 (d, 4H), 2.84 (t, 4H), 2.78 (t, 4H), 1.70 (m, 12H), 1.48–1.26 (m, 72H), 0.97–0.86 (m, 36H). ^{13}C NMR (150 MHz, CDCl$_3$), δ (ppm): 163.21, 147.28, 146.09, 145.96, 141.56, 141.21, 139.28, 139.04, 136.92, 136.90, 136.65, 134.42, 134.19, 133.17, 133.04, 131.66, 129.59, 129.48, 127.79, 125.47, 124.18, 123.37, 121.73, 116.02, 97.55, 68.82, 41.19, 38.79, 34.30, 32.54, 31.93, 31.87, 30.59, 30.40, 30.32, 29.61, 29.55, 29.51, 29.47, 29.41, 29.35, 29.26, 28.94, 28.93, 25.72, 23.76, 23.05, 22.95, 22.71, 22.68, 14.18, 14.13, 14.06, 11.02, 10.92. MS (UHR-TOF): calcd for $C_{114}H_{152}N_2O_4S_{10}$ [M]$^+$, 1932.8959; found, 1932.8962.

Notes and references

1 G. Yu, J. Gao, J. C. Hummelen, F. Wudl and A. J. Heeger, *Science*, 1995, **270**, 1789.
2 Z. B. Henson, K. Müllen and G. C. Bazan, *Nat. Chem.*, 2012, **4**, 699.
3 B. C. Thompson and J. M. Frechet, *Angew. Chem., Int. Ed.*, 2008, **47**, 58.
4 J. Chen and Y. Cao, *Acc. Chem. Res.*, 2009, **42**, 1709.
5 K. Müllen and T. M. Swager, *Acc. Chem. Res.*, 2008, **41**, 1085.
6 J. Hou, H. Y. Chen, S. Zhang, R. I. Chen, Y. Yang, Y. Wu and G. Li, *J. Am. Chem. Soc.*, 2009, **131**, 15586.
7 S. Günes, H. Neugebaue and N. S. Sariciftci, *Chem. Rev.*, 2007, **107**, 1324.
8 X. Zhang, Z. Lu, L. Ye, C. Zhan, J. Hou, S. Zhang, B. Jiang, Y. Zhao, J. Huang, S. Zhang, Y. Liu, Q. Shi, Y. Liu and J. Yao, *Adv. Mater.*, 2013, **25**, 5791.
9 X. Guo, M. Baumgarten and K. Müllen, *Prog. Polym. Sci.*, 2013, **38**, 1832.
10 Z. He, C. Zhong, S. Su, M. Xu, H. Wu and Y. Cao, *Nat. Photon.*, 2012, **6**, 591.
11 D. H. Wang, A. K. K. Kyaw, V. Gupta, G. C. Bazan and A. J. Heeger, *Adv. Energy Mater.*, 2013, **3**, 1161.
12 (*a*) J. Zhou, Y. Zuo, X. Wan, G. Long, Q. Zhang, W. Ni, Y. Liu, Z. Li, G. He, C. Li, B. Kan, M. Li and Y. Chen, *J. Am. Chem. Soc.*, 2013, **135**, 8484; (*b*) Y. Liu, C. Chen, Z. Hong, J. Gao, Y. M. Yang, H. Zhou, L. Dou, G. Li and Y. Yang, *Sci. Rep.*, 2013, **3**, 3356.
13 Y. Sun, G. C. Welch, W. L. Leong, C. J. Takacs, G. C. Bazan and A. J. Heeger, *Nat. Mater.*, 2011, **11**, 44.
14 Y. Liu, Y. M. Yang, C. C. Chen, Q. Chen, L. Dou, Z. Hong, G. Li and Y. Yang, *Adv. Mater.*, 2013, **25**, 4657.
15 Y. Lin, L. Ma, Y. Li, Y. Liu, D. Zhu and X. Zhan, *Adv. Energy Mater.*, 2013, **3**, 1166.
16 A. B. Tamayo, X. D. Dang, B. Walker, J. Seo, T. Kent and T. Q. Nguyen, *Appl. Phys. Lett.*, 2009, **94**, 103301.
17 Y. Chen, X. Wan and G. Long, *Acc. Chem. Res.*, 2013, **46**, 2645.
18 N. M. Kronenberg, M. Deppisch, F. Wurthner, H. W. Lademann, K. Deing and K. Meerholz, *Chem. Commun.*, 2008, 6489.
19 S. Loser, C. J. Bruns, H. Miyauchi, R. P. Ortiz, A. Facchetti, S. I. Stupp and T. J. Marks, *J. Am. Chem. Soc.*, 2011, **133**, 8142.
20 J. Zhou, X. Wan, Y. Liu, Y. Zuo, Z. Li, G. He, G. Long, W. Ni, C. Li, X. Su and Y. Chen, *J. Am. Chem. Soc.*, 2012, **134**, 16345.
21 J. Liu, Y. Sun, P. Moonsin, M. Kuik, C. M. Proctor, J. Lin, B. B. Hsu, V. Promarak, A. J. Heeger and T. Q. Nguyen, *Adv. Mater.*, 2013, **25**, 5898.

15910 | *J. Mater. Chem. A*, 2014, **2**, 15904–15911

This journal is © The Royal Society of Chemistry 2014

22 T. Bura, N. Leclerc, R. Bechara, P. Lévêque, T. Heiser and R. Ziessel, *Adv. Energy Mater.*, 2013, **3**, 1118.

23 H. C. Chen, Y. H. Chen, C. C. Liu, Y. C. Chien, S. W. Chou and P. T. Chou, *Chem. Mater.*, 2012, **24**, 4766.

24 C. Cabanetos, A. E. Labban, J. A. Bartelt, J. D. Douglas, W. R. Mateker, J. M. Frechet, M. D. McGehee and P. M. Beaujuge, *J. Am. Chem. Soc.*, 2013, **135**, 4656.

25 N. Zhou, X. Guo, R. P. Ortiz, S. Li, S. Zhang, R. P. Chang, A. Facchetti and T. J. Marks, *Adv. Mater.*, 2012, **24**, 2242.

26 B. Walker, C. Kim and T. Q. Nguyen, *Chem. Mater.*, 2011, **23**, 470.

27 A. Mishra and P. Bauerle, *Angew. Chem., Int. Ed.*, 2012, **51**, 2020.

28 J. Min, Z. G. Zhang, S. Zhang and Y. Li, *Chem. Mater.*, 2012, **24**, 3247.

29 L. Dou, J. Gao, E. Richard, J. You, C. C. Chen, K. C. Cha, Y. He, G. Li and Y. Yang, *J. Am. Chem. Soc.*, 2012, **134**, 10071.

30 W. Li, W. S. Roelofs, M. M. Wienk and R. A. Janssen, *J. Am. Chem. Soc.*, 2012, **134**, 13787.

31 L. Huo, J. Hou, S. Zhang, H. Y. Chen and Y. Yang, *Angew. Chem., Int. Ed.*, 2010, **49**, 1500.

32 Y. Huang, X. Guo, F. Liu, L. Huo, Y. Chen, T. P. Russell, C. C. Han, Y. Li and J. Hou, *Adv. Mater.*, 2012, **24**, 3383.

33 D. Lee, E. Hubijar, G. J. D. Kalaw and J. P. Ferraris, *Chem. Mater.*, 2012, **24**, 2534.

34 Y. Li, *Acc. Chem. Res.*, 2012, **45**, 723.

35 M. Zhang, Y. Gu, X. Guo, F. Liu, S. Zhang, L. Huo, T. P. Russell and J. Hou, *Adv. Mater.*, 2013, **25**, 4944.

36 D. Patra, T. Y. Huang, C. C. Chiang, R. O. V. Maturana, C. W. Pao, K. C. Ho, K. H. Wei and C. W. Chu, *ACS Appl. Mater. Interfaces*, 2013, **5**, 9494.

37 G. Wei, S. Wang, K. Sun, M. E. Thompson and S. R. Forrest, *Adv. Energy Mater.*, 2011, **1**, 184.

38 W. L. Leong, G. C. Welch, J. Seifter, J. H. Seo, G. C. Bazan and A. J. Heeger, *Adv. Energy Mater.*, 2013, **3**, 356.

39 G. Li, R. Zhu and Y. Yang, *Nat. Photon.*, 2012, **6**, 153.

40 J. A. Love, C. M. Proctor, J. Liu, C. J. Takacs, A. Sharenko, T. S. van der Poll, A. J. Heeger, G. C. Bazan and T. Q. Nguyen, *Adv. Funct. Mater.*, 2013, **23**, 5019.

41 H. Zhou, L. Yang and W. You, *Macromolecules*, 2012, **45**, 607.

42 Z. Li, J. Pei, Y. Li, B. Xu, M. Deng, Z. Liu, H. Li, H. Lu, Q. Li and W. Tian, *J. Phys. Chem. C*, 2010, **114**, 18270.

43 S. Zeng, L. Yin, C. Ji, X. Jiang, K. Li, Y. Li and Y. Wang, *Chem. Commun.*, 2012, **48**, 10627.

44 M. C. Scharber, D. Mühlbacher, M. Koppe, P. Denk, C. Waldauf, A. J. Heeger and C. J. Brabec, *Adv. Mater.*, 2006, **18**, 789.

45 Y. Chen, Z. Du, W. Chen, Q. Liu, L. Sun, M. Sun and R. Yang, *Org. Electron.*, 2014, **15**, 405.

46 C. J. Brabec, C. Winder, N. S. Sariciftci, J. C. Hummelen, A. Dhanabalan, P. A. van Hal and R. A. J. Janssen, *Adv. Funct. Mater.*, 2002, **12**, 709.

47 A. Gadisa, M. Svensson, M. R. Andersson and O. Inganas, *Appl. Phys. Lett.*, 2004, **84**, 1609.

48 G. G. Malliaras, J. R. Salem, P. J. Brock and C. Scott, *Phys. Rev. B: Condens. Matter Mater. Phys.*, 1998, **58**, 13411–13414.

49 X. Hu, L. Zuo, W. Fu, T. T. Larsen-Olsen, M. Helgesen, E. Bundgaard, O. Hagemann, M. Shi, F. C. Krebs and H. Chen, *J. Mater. Chem.*, 2012, **22**, 15710.

50 V. D. Mihailetchi, J. Wildeman and P. W. Blom, *Phys. Rev. Lett.*, 2005, **94**, 126602.

51 Z. Bao, A. J. Lovinger and A. Dodabalapur, *Appl. Phys. Lett.*, 1996, **69**, 3066.

52 M. He, W. Han, J. Ge, W. Yu, Y. Yang, F. Qiu and Z. Lin, *Nanoscale*, 2011, **3**, 3159.

53 U. Zhokhavets, T. Erb, G. Gobsch, M. Al-Ibrahim and O. Ambacher, *Chem. Phys. Lett.*, 2006, **418**, 347.

54 J. Liu, H. Choi, J. Y. Kim, C. Bailey, M. Durstock and L. Dai, *Adv. Mater.*, 2012, **24**, 538.

55 C. T. Lee, W. T. Yang and R. G. Parr, *Phys. Rev. B: Condens. Matter Mater. Phys.*, 1988, **37**, 785.

56 A. D. Becke, *J. Chem. Phys.*, 1993, **98**, 5648.

57 W. J. Hehre, R. Ditchfield and J. A. Pople, *J. Chem. Phys.*, 1972, **56**, 2257.

58 P. C. Harihara and J. A. Pople, *Theor. Chim. Acta*, 1973, **28**, 213.

59 L. X. Chen, S. Xiao and L. Yu, *J. Phys. Chem. B*, 2006, **110**, 11730.

60 L. Huo, S. Zhang, X. Guo, F. Xu, Y. Li and J. Hou, *Angew. Chem., Int. Ed.*, 2011, **50**, 9697.